Journal of Power Sources 262 (2014) 344–348

Contents lists available at ScienceDirect

Journal of Power Sources

journal homepage: www.elsevier.com/locate/jpowsour

Short communication

High-performance supercapacitor electrode based on amorphous mesoporous $Ni(OH)_2$ nanoboxes

Yan Fu [a], Jinmei Song [b,c], Youqi Zhu [a], Chuanbao Cao [a,*]

[a] Research Center of Materials Science, Beijing Institute of Technology, Beijing 100081, PR China
[b] Beijing Composite Materials Co., Ltd, Beijing 102101, PR China
[c] Beijing University of Chemical Technology, Beijing 100029, PR China

HIGHLIGHTS

- Amorphous $Ni(OH)_2$ nanoboxes was prepared by template method.
- $Ni(OH)_2$ nanoboxes has a high surface area of 214.6 m^2 g^{-1}.
- Exhibited high specific capacitance of 2495, 1993 F g^{-1} at current of 1 and 10 A g^{-1}.
- Uniform hollow and mesoporous structure contribute to excellent performance of supercapacitor.

ARTICLE INFO

Article history:
Received 16 December 2013
Received in revised form
28 February 2014
Accepted 2 April 2014
Available online 8 April 2014

Keywords:
Amorphous
Mesoporous
$Ni(OH)_2$
Supercapacitor

ABSTRACT

Amorphous mesoporous $Ni(OH)_2$ nanoboxes are synthesized by template-engaged routes. The nanoboxes are characterized by SEM, TEM, XRD, XPS and BET methods. The nanoboxes have uniform morphology of 450–500 nm, high surface area of 214.6 m^2 g^{-1} and mesoporous structure of 4–20 nm. Electrochemical characterization are tested using cyclic voltammetry, chronopotentiometry and impedance spectroscopy, respectively. These amorphous mesoporous $Ni(OH)_2$ hollow nanoboxes shows high specific capacitance of 2495, 2378, 2197, 1993 F g^{-1} at discharge current of 1, 2, 5 and 10 A g^{-1} respectively. The property tests demonstrate the high specific capacitance and excellent cycling of the amorphous $Ni(OH)_2$ nanoboxes material for high-performance electrochemical pseudocapacitors.

1. Introduction

Electric energy storage devices with high energy storage capacity and fast charge–discharge ability are very important and desirable today as they can find numerous applications in plug-in electric vehicles, back-up power sources, energy storage for wind and solar energy and so forth. Presently the two major areas of advanced energy storage devices are batteries and electrochemical capacitors [1]. Electrochemical capacitors, also known as supercapacitors, are particularly suitable for applications requiring high power density and high charge–discharge rates, such as portable electronic devices, hybrid vehicles and renewable energy systems, due to their much higher power densities than conventional secondary batteries and their long cycle-life (up to 10^4 cycles) and safety tolerance to high rate charge and discharge [1–4].

The supercapacitors in general include traditional double-layer supercapacitors and Faradic redox reaction pseudocapacitors. The energy density based on pseudo-Faradic processes is usually many times greater than that of the double-layer supercapacitors [5–9]. Transition metal oxides [7,8] and conductive polymers [10–12] are frequently used as the Faradic redox pseudocapacitors. In particular, supercapacitors based on ruthenium oxide have shown ultrahigh pseudocapacitance and excellent reversibility [13,14]. However, the high cost of RuO_2 and the relatively low specific capacitance of NiO_x, CoO_x, and MnO_2 greatly undermine their overall effectiveness for supercapacitor applications [15–22]. Among numerous active electrode materials, nickel hydroxide ($Ni(OH)_2$) has been recognized as a promising electrode material in electrochemical capacitors [9,23].

Regulating and controlling the structure (shape, size or component) of nanomaterials has been already regarded as a challenging but vital work for scientists since the properties of the nanomaterials are usually structure-dependent [24]. In past work, nickel hydroxide with different morphologies have been studied.

* Corresponding author. Tel.: +86 10 68913792; fax: +86 10 68912001.
E-mail address: cbcao@bit.edu.cn (C. Cao).

http://dx.doi.org/10.1016/j.jpowsour.2014.04.002
0378-7753/

Due to their well-defined interior voids, high specific surface area, low density, and structural stability, hollow nanostructures have attracted growing interest in recent years and they should deserve more attention on controllable preparation because of their widely application [25]. In addition, amorphous $Ni(OH)_2$ materials are usually assessed as unsuitable electrochemical capacitors because of their poor performance [26]. However, the amorphous phase offers a rather unique electrochemical behavior [27–29] that may be exploitable in certain device applications. Also, H. B. Li [30] recently report that amorphous nickel hydroxide nanospheres exhibits high capacitance and high energy density. So our study focus on the supercapacitor electrode properties of amorphous $Ni(OH)_2$ nanoboxes.

In our study, we synthesize uniform amorphous $Ni(OH)_2$ nanoboxes using template-engaged routes [31] and then fabricate supercapacitors from these nanoboxes. These mesoporous hollow nanoboxes can greatly increase the specific surface area, thus contributing to the pseudo-capacitance reaction and improving the electrochemical properties of materials. Our measurements indicate that these nanoboxes exhibit excellent overall electrochemical performances, including high capacitance and super-long cycle life. Moreover, this amorphous structure further promotes the application of amorphous-phase nanomaterials as advanced electrochemical pseudocapacitor materials.

2. Experimental

2.1. Preparation of Cu_2O templates and amorphous $Ni(OH)_2$ nanoboxes

10.0 mL NaOH aqueous solution (2.0 mol L^{-1}) was added dropwise into the $CuCl_2 \cdot 2H_2O$ (0.01 mol L^{-1}, 100 mL) transparent light green solution. After stirring for 0.5 h, an ascorbic acid solution (0.6 mol L^{-1}, 10.0 mL) was added dropwise into the dark brown solution. A turbid red liquid gradually formed. The mixture was aged for 3 h, Cu_2O templates were formed. All of these procedures were carried out under constant stirring and heated in a water bath at 40 °C.

Uniform amorphous $Ni(OH)_2$ nanoboxes with intact shell structures were quickly fabricated by deliberately selecting $S_2O_3^{2-}$ as the coordinating etchant toward Cu_2O templates and optimizing the reaction conditions according the previously reported method. [31] 0.1 g Cu_2O templates, 0.034 g $NiCl_2 \cdot 6H_2O$ and 3.33 g PVP were added into 100 mL $CH_3CH_2OH/H_2O = 1{:}1$ solution. After string for 10 min, 40.0 mL $Na_2S_2O_3$ (1.0 mol L^{-1}) was added dropwise into the mixture. $Ni(OH)_2$ nanoboxes were formed after string for 10 min.

2.2. Characteration of amorphous $Ni(OH)_2$ nanoboxes

The morphology and microstructure of the as-prepared amorphous $Ni(OH)_2$ nanoboxes were investigated using an FE-SEM (JSM-6701F). Chemical compositions and crystallite structures of the samples were determined by XRD (X0 Pert Pro, Philips). The surface chemical species of the as-prepared amorphous $Ni(OH)_2$ nanoboxes were examined on a PerkineElmer PHI-5702 multifunctional X-ray photoelectron spectroscope (XPS, Physical Electronics, USA) using Al Kα radiation of 1486.6 eV as the excitation source. Nitrogen adsorption–desorption isotherm measurements were performed on a Micromeritics ASAP 2020 volumetric adsorption analyzer at 77 K. Before adsorption–desorption isotherm measurements, the samples were outgassed at 80 °C for 10 h in the degas port of the analyzer. The Brunauer–Emmette Teller (BET) method was utilized to calculate the specific surface area of the sample.

2.3. Electrode preparation and electrochemical measurements

The working electrode was prepared by mixing the electroactive material ($Ni(OH)_2$, 80 wt%), 10 wt% carbon black(10 wt%), and polyvinylidene fluoride (10 wt%). The mixture was then pressed onto a nickel grid and dried at 80 °C in air for 3 h. Each electrode contained about 1–2 mg of electroactive material. The electrochemical performance of the $Ni(OH)_2$ sample was evaluated by using a three-electrode cell with Pt foil as the counter electrode and a saturated calomel electrode (SCE) as the reference electrode in 2 M KOH aqueous solution. Cyclic voltammograms (CVs) were measured on a Parstat 2273 advanced electrochemical system. Galvanostatic charge–discharge tests were carried out on an Arbin BT2000 system in the voltage range of 0–0.5 V (vs. SCE) under different current densities.

3. Results and discussion

3.1. Morphology of amorphous $Ni(OH)_2$ nanoboxes

The typical low-magnification scanning electron microscopy (SEM) image (Fig. 1(a)) clearly illustrates the as-synthesized samples be composed of many well-defined nanoboxes. An overview scanning electron microscopy (SEM) image in Fig. 1(a) shows that

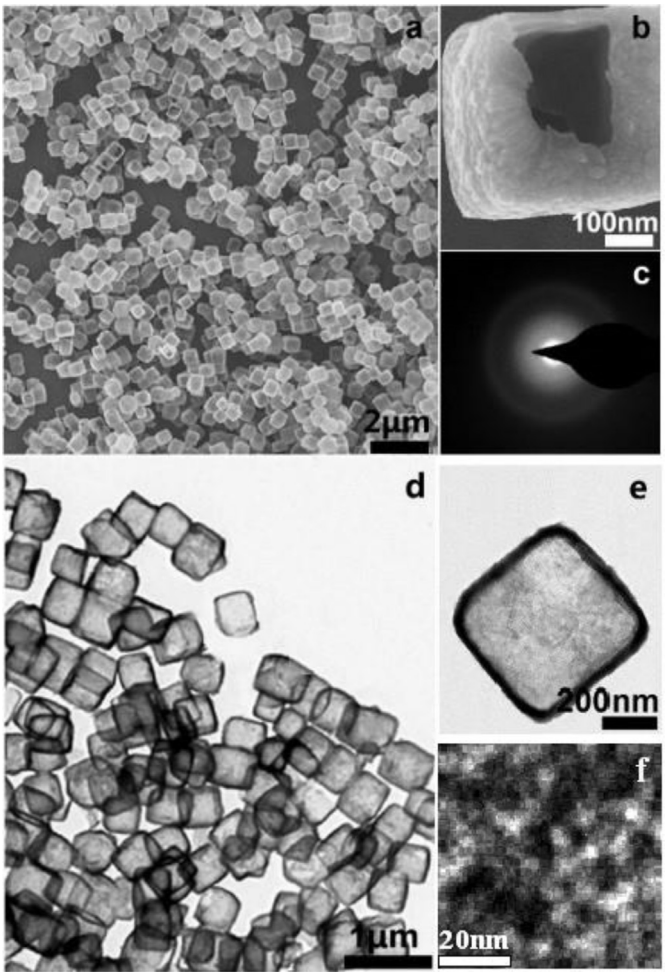

Fig. 1. (a) overview SEM image of the sample with uniform morphology (b) magnified SEM image of a nanobox $Ni(OH)_2$ nanoboxes (c) the SAED pattern of the nanobox; (d) TEM image of the as-prepared $Ni(OH)_2$ nanoboxes; e) a typical nanobox with well-defined interior and very thin shell; (f) mesopores structure of a nanobox.

the sample consists of uniform nanoboxes without impure particles or aggregates. A cracked nanobox as shown in Fig. 1(b), interior space can be seen directly. The as-prepared $Ni(OH)_2$ nanoboxes have a hollow interior and architecture. The cleft of these nanoboxes might be caused by rapid mass transport across the shells during fast dissolution of the Cu_2O. No crystalline morphology is detected in the bright-field transmission electron microscopy (TEM) image of the sample (Fig. 1(c)). The selected area electron diffraction (SAED) pattern suggests the amorphous feature of the nanoboxes. The as-prepared $Ni(OH)_2$ nanoboxes are further studied by TEM images. As displayed in Fig. 1(d), a highly uniformity of the nanoboxes can be observed from the image, which is in agreement with the SEM findings in Fig. 1(a). The TEM image (Fig. 1(e)) clearly illustrates small particles constitute the cubic shell structure with the edge length of 450–500 nm. The shell of the nanoboxes is as thin as about 35–45 nm owing to the initial low amount of Ni^{2+} in solution. As displayed in Fig. 1(f), the mesopores of a nanobox can be observed. The mesopores sizes are differed. The mesopore structure could be the main cause for high specific surface area of the nanoboxes.

3.2. Crystallographic structure of as-prepared $Ni(OH)_2$ nanoboxes

The crystallographic structure and phase purity of $Ni(OH)_2$ nanoboxes are evaluated by X-ray powder diffraction (XRD) as shown in Fig. 2. The sample appears its amorphous feature both before and after electrochemical properties test. It shows the amorphous structure of $Ni(OH)_2$ nanoboxes never change after electrochemical test, which will lead to excellent cycling performance.

3.3. Chemical compositions of amorphous $Ni(OH)_2$ nanoboxes

XPS is an effective surface chemical analysis technique, which is used to determine the species and chemical states of the elements in the surface of the materials. The X-ray photoelectron spectroscopy (XPS) of the product is shown in Fig. 3. It is observed that a main peak at 856.1 eV in $Ni_{2p\ 3/2}$ spectrum, with satellite peaks due to Plasmon losses and final state effects [31,32]; and a single peak at 530.8 eV in O_{1s} spectrum. By comparing the data with previous XPS studies on Ni, NiO, NiOOH, and $Ni(OH)_2$, the presented $Ni_{2p3/2}$ and O_{1s} spectrums can be assigned to Ni^{2+} and OH^-, respectively, in $Ni(OH)_2$ [33,34]. Hence, it is clear that $Ni(OH)_2$ is formed under the present experimental conditions.

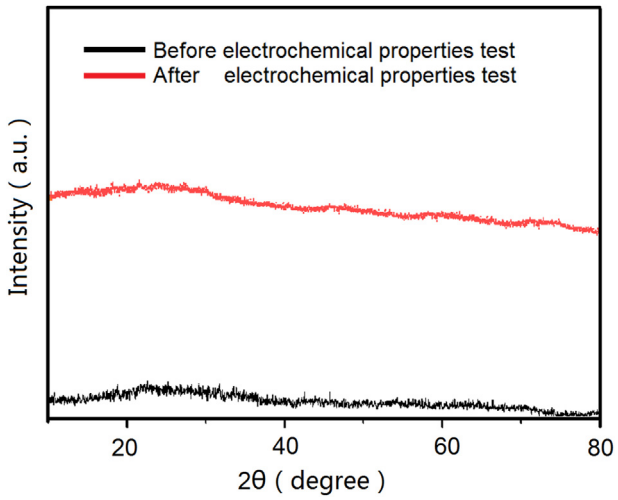

Fig. 2. XRD pattern of the $Ni(OH)_2$ nanoboxes, before and after electrochemical properties test (1 mV s^{-1}, 1000 cycling) respectively.

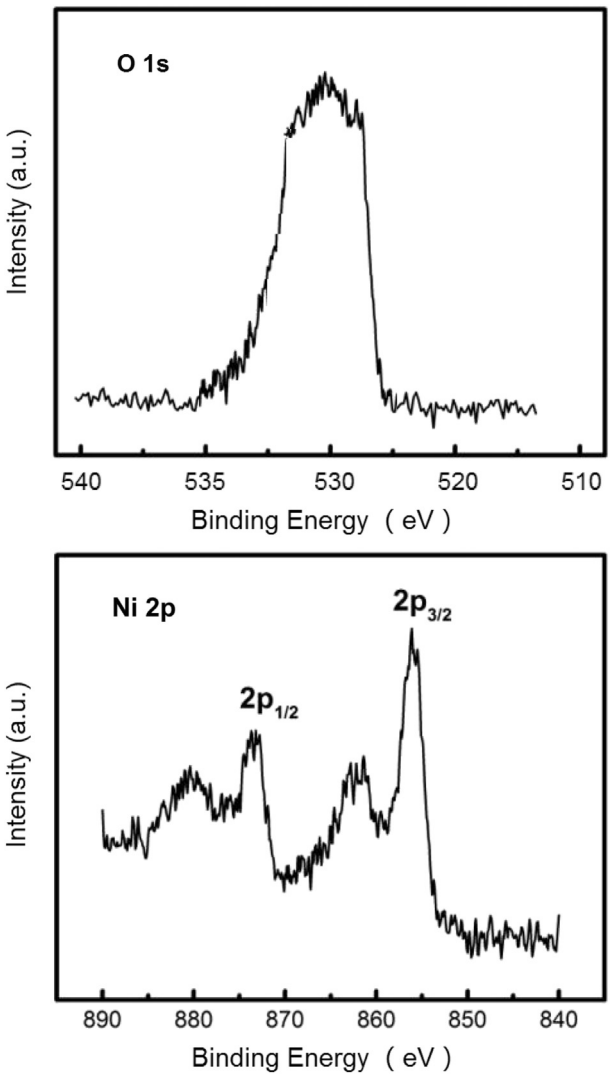

Fig. 3. XPS results of the as-prepared sample.

3.4. BET properties of amorphous $Ni(OH)_2$ nanoboxes

Fig. 4(b) shows the pore diameter distributions of the sample. As shown in this figure, the $Ni(OH)_2$ materials possess a mesoporous distribution at around 4–20 nm. A sharp pore size distribution with an average pore size of 9 nm was obtained by BJH method, calculated through the desorption isotherm. Since the size range of the hydrated ions in the electrolyte is typically 6–7.6 Å, and the pore size at the range of 8–50 Å is the effective one required to increase either the pseudo-capacitance or electric double-layer capacitance [35].

Special high BET surface area and the effective distributions of the pore size of the nanobox-like nanostructures provides the possibility of efficient transport of electrons and ions in supercapacitors, which will lead to high electrochemical capacity.

3.5. Electrochemical performance of the armorphous $Ni(OH)_2$ nanoboxes

The electrochemical performances of the amorphous $Ni(OH)_2$ hollow nanoboxes as electrode materials for supercapacitors are tested using cyclic voltammograms (CVs) and galvanostatic charge–discharge (GCD) in 2 M KOH aqueous solution in the

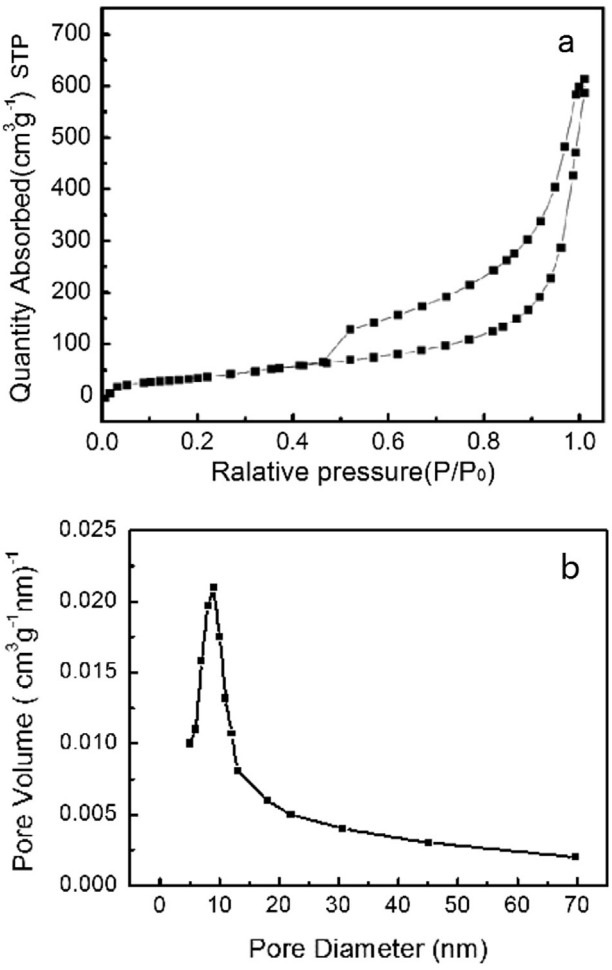

Fig. 4. The typical N_2 adsorption–desorption isotherm of amorphous $Ni(OH)_2$ nanoboxes.

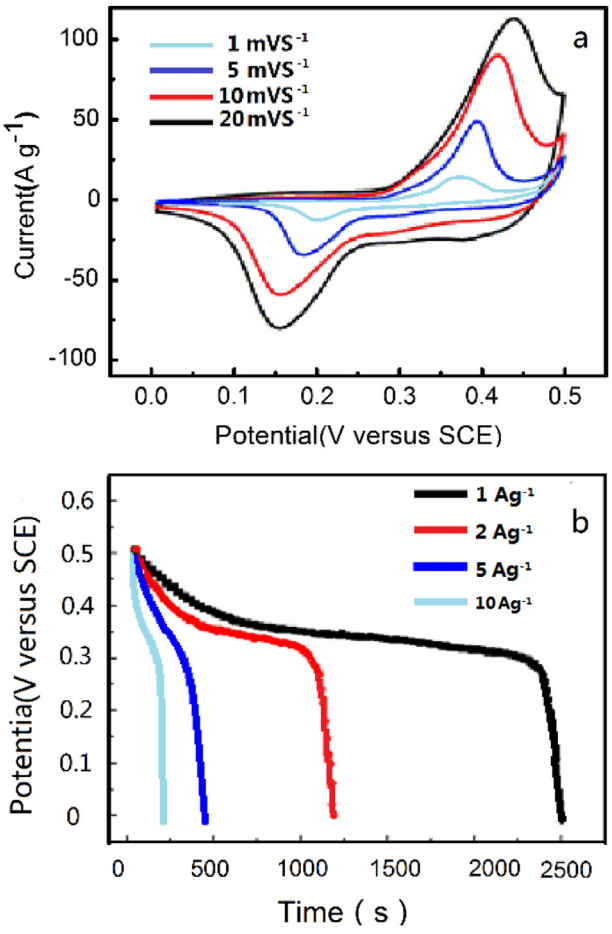

Fig. 5. Electrochemical characterization of amorphous $Ni(OH)_2$ nanoboxes electrode. (a) CV curves of the amorphous $Ni(OH)_2$ nanoboxes at various scan rates in 2 M KOH. (b) Discharge curves of amorphous $Ni(OH)_2$ nanoboxes at various current densities (ranging from 1 to 10 A g^{-1}).

potential range 0–0.5 V vs. SCE. Fig. 5(a) shows the CV curves of the amorphous $Ni(OH)_2$ nanoboxes electrode at different scan rates. The shape of the CV reveal that the capacitance characteristic is very different from that of traditional electric double-layer capacitance in which the shape is normally an ideal rectangular shape. A pair of cathodic and anodic peaks is observed in the CV curves. This result, corroborating previous reports [36–38] indicates the occurrence of Faradaic reactions which is based on the reversible redox mechanism in the amorphous $Ni(OH)_2$. The mass of the as-synthesized $Ni(OH)_2$ nanoboxes is 0.1179 mg cm^{-2}. Therefore, the specific capacitances of the amorphous $Ni(OH)_2$ samples are calculated to be 2401, 1689, 1497, 1400 and 1238 F g^{-1} at scan rates of 1, 5, 10, 15 and 20 mV s^{-1}, respectively. With increasing scan rate, the specific capacitance decreases gradually, which can be attributed to electrolytic ions diffusing and migrating into the active materials at low scan rates. At high scan rates, the diffusion effect, limiting the migration of the electrolytic ions, causes some active surface areas to become inaccessible for charge storage [30]. This result indicates the excellent capacitive behavior and high-rate capability of the amorphous phase. Note that the measured capacitance of the amorphous uniform $Ni(OH)_2$ nanosboxes is higher than that of reported amorphous $Ni(OH)_2$ nanospheres material [30] 2188 F g^{-1},1667 F g^{-1} at the scan rates of 1 and 5 mV s^{-1}, respectively. This high specific capacitance can mainly attributed to the high surface area and mesoporous hollow nanostructure, which provide effective diffusion channels for the electrolyte ions.

Fig. 5(b) shows the results obtained for the $Ni(OH)_2$ nanoboxes electrode in the potential range of 0–0.5 V at various discharging current densities. The specific capacitance of the electrode can be calculated from the discharge curve. The specific capacitances are calculated from the galvanostatic discharge curves to be 2495, 2378, 2197 and 1993 F g^{-1} at discharge current of 1, 2, 5 and 10 A g^{-1}, respectively. The discharge capacitance at 10 A g^{-1} is still about 80% of that discharge current at 1 A g^{-1}. Clearly, the specific capacitance slightly decreases with increasing current density. In particular, the mesoporous structures can act as “ion reservoirs”, which provides steady supply of OH^- ions and ensure that Faradic reactions take place efficiently at high current densities for energy storage [39].

Stability over repeated charge and discharge cycling is critical for supercapacitors in practice. A charge–discharge cycling test is carried out to examine the stability of amorphous $Ni(OH)_2$ nanoboxes electrode at different current densities (1–10 A g^{-1}) between 0 and 0.5 V (vs. SCE) in 2 M KOH electrolyte. As shows in Fig.6, the current density from 1 A g^{-1} to 10 A g^{-1} results in the reduction in the specific capacitance from 2495 F g^{-1} to 1993 F g^{-1}. The capacity of the electrode is still maintain about 98.5% of the initial capacity after 100 cycle's 1 A g^{-1}, 100 cycle's 2 A g^{-1}, 100 cycle's 5 A g^{-1} and 100 cycle's 10 A g^{-1} test. It is illustrates the preparation of

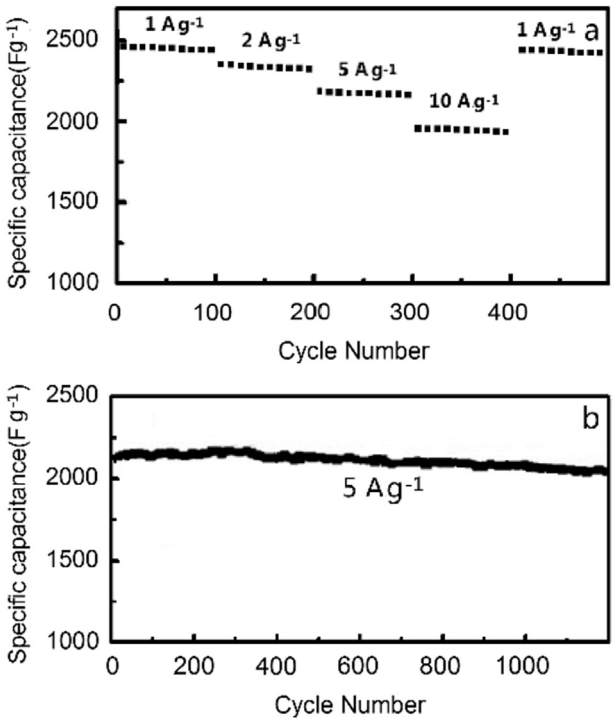

Fig. 6. Cycling performance of as-prepared $Ni(OH)_2$ hollow nanobox electrode in 2 M KOH electrolyte: (a) at different current densities and (b) at a discharge current of 5 A g^{-1}.

amorphous $Ni(OH)_2$ nanoboxes electrode have good rate performance and cycle stability.

The cyclability of the amorphous $Ni(OH)_2$ nanoboxes is further tested by continuous charge–discharge measurements (Fig. 6(b)) over 1200 cycles at a current density of 5 A g^{-1}. The specific capacitances increases during the first several cycles, which is possibly due to the activation process of the $Ni(OH)_2$ electrode. After this process, the specific capacitances are stable at about 2100 F g^{-1}, losing less than 5% capacitance at the end of the test.

Good rate performance and the cycle stability of the amorphous $Ni(OH)_2$ nanoboxes may due to its morphology, the mesoporous structure. One reason is the hollow nanoboxes structure and the mesoporous provides more penetration and migration through the electrode surface road. The other reason is the nanoboxes have good hydrophilicity because the preparation reaction of $Ni(OH)_2$ nanoboxes was carried in aqueous solution. Good hydrophilicity is beneficial to the electrolyte in the electrode surface diffusion and migration.

4. Conclusion

In summary, amorphous $Ni(OH)_2$ hollow nanoboxes precursors are produced by a template method. The samples have a uniform morphology, a high surface area of 214.6 m^2 g^{-1} and a mesoporous structure of 4–20 nm. The high specific surface area and mesoporous structure are favorable for the pseudo-capacitance reaction and improve the electrochemical properties of materials. The results demonstrate the high specific capacitance and excellent cycling property of the amorphous $Ni(OH)_2$ nanoboxes material for high-performance electrochemical pseudocapacitors. These amorphous $Ni(OH)_2$ hollow nanoboxes show high specific capacitance of 2495, 2378, 2197, 1993 F g^{-1} at discharge current of 1, 2, 5 and 10 A g^{-1} respectively. After continuous charge–discharge measurements over 1200 cycles at a current density of 5 A g^{-1}, the specific capacitances are still maintained at about 2100 F g^{-1}, only losing less than 5% capacitance at the end of the test.

Acknowledgments

This work was financially supported by the National Natural Science Foundation of China (Grant No. 21371023).

References

[1] B.E. Conway, Electrochemical Capacitors: Scientific Fundamentals and Technological Applications, Kluwer Academic/Plenum, New York, 1999.
[2] M. Winter, R.J. Brodd, Chem. Rev. 104 (2004) 4245–4269.
[3] Antonino Salvatore Aricò, Peter Bruce, Bruno Scrosati, Jean-Marie Tarascon, Walter van Schalkwijk, Nat. Mater. 4 (2005) 366–377.
[4] Yu-Guo Guo, Jin-Song Hu, Li-Jun Wan, Adv. Mater. 20 (2008) 2878–2887.
[5] R. Liu, S.B. Lee, J. Am. Chem. Soc. 130 (2008) 2942–2943.
[6] K.R. Prasad, K. Koga, N. Miura, Chem. Mater. 16 (2004) 1845–1847.
[7] C. Yu, L. Zhang, J. Shi, J. Zhao, J. Gao, D. Yan, Adv. Funct. Mater. 18 (2008) 1544–1554.
[8] T. Zhu, J.S. Chen, X.W. Lou, J. Mater. Chem. 20 (2010) 7015–7020.
[9] H. Wang, H.S. Casalongue, Y. Liang, H. Dai, J. Am. Chem. Soc. 132 (2010) 7472–7477.
[10] M.E. Roberts, D.R. Wheeler, B.B. McKenzie, B.C. Bunker, J. Mater. Chem. 19 (2009) 6977–6979.
[11] Y. Fang, J. Liu, D.J. Yu, J.P. Wicksted, K. Kalkan, C.O. Topal, B.N. Flanders, J. Wu, J. Li, J. Power Sources 195 (2010) 674–679.
[12] K. Zhang, L.L. Zhang, X.S. Zhao, J. Wu, Chem. Mater. 22 (2010) 1392–1401.
[13] R.R. Bi, X.L. Wu, F.F. Cao, L.Y. Jiang, Y.G. Guo, L.J. Wan, J. Phys. Chem. C 114 (2010) 2448–2451.
[14] Y.F. Ke, D.S. Tsai, Y.S. Huang, J. Mater. Chem. 15 (2005) 2122–2127.
[15] J.P. Zheng, P.J. Cygan, T.R. Zow, J. Electrochem. Soc. 142 (1995) 2699–2703.
[16] Y.G. Wang, Z.D. Wang, Y.Y. Xia, Electrochim. Acta 50 (2005) 5641–5646.
[17] C. Lin, J.A. Ritter, B.N. Popov, Electrochem. Soc. 145 (1998) 4097–4103.
[18] L.B. Kong, J.W. Lang, M. Liu, Y.C. Luo, L. Kang, J. Power Sources 194 (2009) 1194–1201.
[19] S.C. Pang, M.A. Anderson, T.W. Chapman, J. Electrochem. Soc. 147 (2000) 444–450.
[20] K.C. Liu, M.A. Anderson, J. Electrochem. Soc. 143 (1996) 124–130.
[21] V. Srinivasan, J.W. Weidner, J. Electrochem. Soc. 144 (1997) L210–L213.
[22] K.W. Nam, K.B. Kim, J. Electrochem. Soc. 149 (2002) A346–A354.
[23] T.N. Ramesh, R.S. Jayashree, P.V. Kamath, S. Rodrigues, A.K. Shukla, J. Power Sources 104 (2003) 295–298.
[24] Mostafa A. El-Sayed, Acc. Chem. Res. 37 (2004) 326–333.
[25] X.W. Lou, L.A. Archer, Z. Yang, Adv. Mater. 20 (2008) 3987–4019.
[26] C.J. Liu, Y.W. Li, J. Alloys Compd. 478 (2009) 415–418.
[27] H. Zhang, et al., Nano Lett. 8 (2008) 2664–2668.
[28] S. Devaraj, N. Munichandraiah, J. Phys. Chem. C 112 (2008) 4406–4417.
[29] L. Mao, K. Zhang, H.S.O. Chan, J.S. Wu, J. Mater. Chem. 22 (2012) 1845–1851.
[30] H.B. Li, M.H. Yu, F.X. Wang, P. Liu, Y. Liang, J. Xiao, C.X. Wang, Y.X. Tong, G.W. Yang, Nat. Commun. 4 (2013) 1894–1901.
[31] Jianwei Nai, Shuqian Wang, Yang Bai, Lin Guo, Small (2013) 3147–3152.
[32] N.S. McIntyre, M.G. Cook, Anal. Chem. 47 (1975) 2208–2213.
[33] B.P. Payne, M.C. Biesinger, N.S. McIntyre, J. Electron Spectrosc. Relat. Phenom. 175 (2009) 55–65.
[34] M.C. Biesinger, B.P. Paynec, L.W.M. Lau, A. Gerson, R. St. C. Smart, Surf. Interface Anal. 41 (2009) 324–332.
[35] L. Cao, M. Lu, H.L. Li, J. Electrochem. Soc. 152(5) (2005) A871–A875.
[36] G.W. Yang, C.L. Xu, H.L. Li, Chem. Commun. (2008) 6537–6539.
[37] Y.F. Yuan, et al., Electrochim. Acta 56 (2011) 2627–2632.
[38] H.L. Li, et al., Electrochim. Acta 58 (2011) 89–94.
[39] D.W. Wang, F. Li, M. Liu, G. Lu, H.M. Cheng, Angew. Chem. Int. Ed. 48 (2009) 1515–1526.